Supplementary Information

Efficient *in vivo* wound healing using noble metal nanoclusters

Kuo Li[a, †], Dan Li[a, †], Cheng-Hsuan Li[b], Pengfei Zhuang[a], Chunmei Dai[a], Xiangka Hu[a], Dahao Wang[a], Yuanye Liu[a], Xifan Mei[a], Vincent M. Rotello[b]**

[a]Department of Orthopedics, The First Affiliated Hospital of Jinzhou Medical University, 40 Songpo Road, Jinzhou, China 121001, China

[b]Department of Chemistry, University of Massachusetts Amherst, 710 North Pleasant Street, Amherst, Massachusetts 01003, USA

Corresponding authors

*E-mail: meixifan@jzmu.edu.cn

*E-mail: rotello@chem.umass.edu

Table of contents

1. Experimental Methods

Calorimetric experiment. Bacteria were cultured in Lysogeny broth (LB) medium at 37 °C in a shaker. The bacterial cells were cultured on LB agar. For each experiment, a single colony of bacteria was picked from the fresh LB agar plate and cultured at 37 °C for ca. 12 h. Then, the cultured bacteria were introduced to the fresh LB medium at the initial concentration (OD 600) of ca. 1.0×10^8 CFU /mL. The ampoules containing the bacterial cell suspension in the presence and absence of NCs were sealed up and put into eight-channel calorimeter blocks. When the curve returned to the baseline and stabilized, the measurement was ended. A TAM air isothermal calorimeter with ampoule mode was used to measure the growth of *E. coli* and *S. aureus*. The NCs (100 μM/mL) was added to each glass ampoule respectively. The glass ampoule was then sealed with a lid and placed in a microcalorimeter at 37 °C.

Immunofluorescence. HUVECs were adhered to 96-well plates for 24 hours at 37 ° C with 5% CO_2 (cell count, ~ 4×10^5). Cells without the addition of NCs were used as a control. The cells were treated with 100 μM of NCs in each group, the cells were washed three times with PBS after incubation 24 hours. Subsequently, the cells were fixed, perforated, and then sealed with 5% goat serum for 2 h. After that, these cells were respectively incubated overnight with primary antibody Tubulin antibody, NF-κB antibody, and IL-1β antibody at 4 °C. Then, the cells were washed with PBS three times. Subsequently, these cells were cultured with appropriate secondary antibodies for 2 h and washed with PBS three times. Finally, the cells were stained with DAPI for 15 minutes and washed three times with PBS. The fluorescence intensity is read by the Microreader and the cell imaging was studied by fluorescence microscopy.

Biosafety study. Rats were randomly divided into different groups (4 rats in each group). Afterwards, rats were injected intraperitoneally with 0.2 mL NaCl (0.9%) or 0.2 mL DHLA-AuNCs (100 μM). rats were euthanized on days 1 and 12 to obtain samples of their organs including the heart, liver, kidney, and spleen. After that, those organ samples were embedded by wax block and further sliced, and dewaxed. The sections were stained with H&E (Sigma-Aldrich, St. Louis, MO). At the same time, a routine blood test of all rat was performed before and after the injection of NCs.

ROS detection at abiotic conditions. A stock solution of the 2′, 7′-Dichlorofluorescin diacetate (DCFH-DA) probe was made by dissolving DCFH-DA powder into dimethyl sulfoxide (DMSO reagent). The deacetylation of DCFH-DA was carried out by adding a strong base of sodium hydroxide (NaOH). This solution was kept in darkness at room temperature (25 °C) for 30 min. The working solution was prepared by dilution with a 10 mM phosphate (PB) buffer (pH 7.2). The ROS at abiotic conditions was produced by using a mixture of AuNCs and H_2O_2. In a 1.5 mL Eppendorf (EP) tube, 500 μL of 0.03% H_2O_2 was mixed with AuNCs of different concentrations (0 μM, 1 μM, 5 μM, 10 μM, 20 μM, 50 μM, 100 μM, and 200 μM) respectively for 1 hour. Then 100 μL of the mixtures were transferred to 96-well plates. Finally, 10 μL of DCFH-DA probes (10 μM) were combined with each mixture in the well and incubated for 30 minutes. A control blank

was obtained by adding the same amount of PB to the H_2O_2 solutions. All mixtures were incubated for 30 min at 37 °C before testing. The fluorescence images of the mixtures were investigated by a microscope (Leica DMI 4000 B) with maximum excitation and emission spectra of 485 nm and 535 nm respectively.

2. TEM of NCs

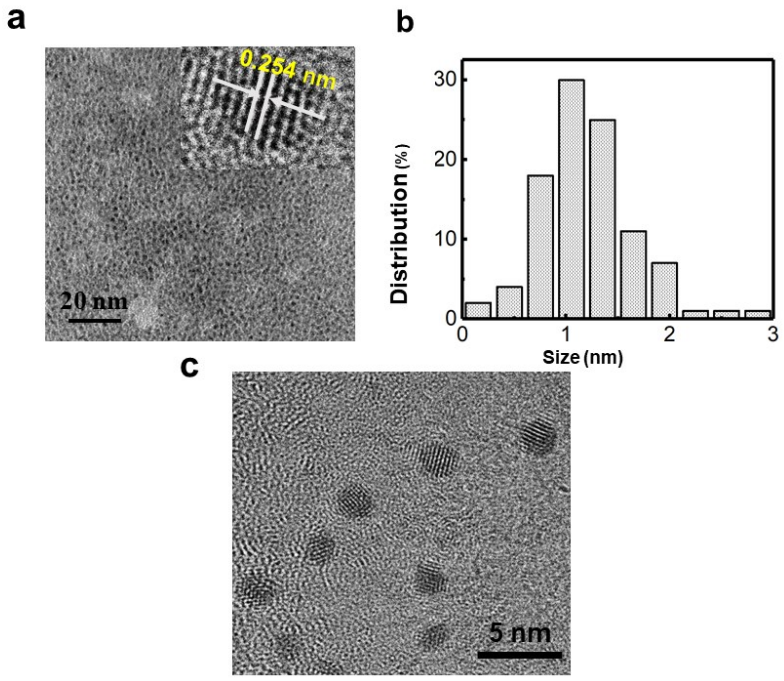

Figure S1 (a) Low magnification transmission electron microscopy (TEM) image, showing small size (ca. 1.2 nm) GSH-AgNCs; The inset of (a) shows well-resolved lattice fringes with measured spacing value "d" value of AgNCs. (b) The size distribution of GSH-AgNCs measured based on the statics of 100 particles. (c) Higher magnification TEM image, which reveals the lattice of the AgNCs.

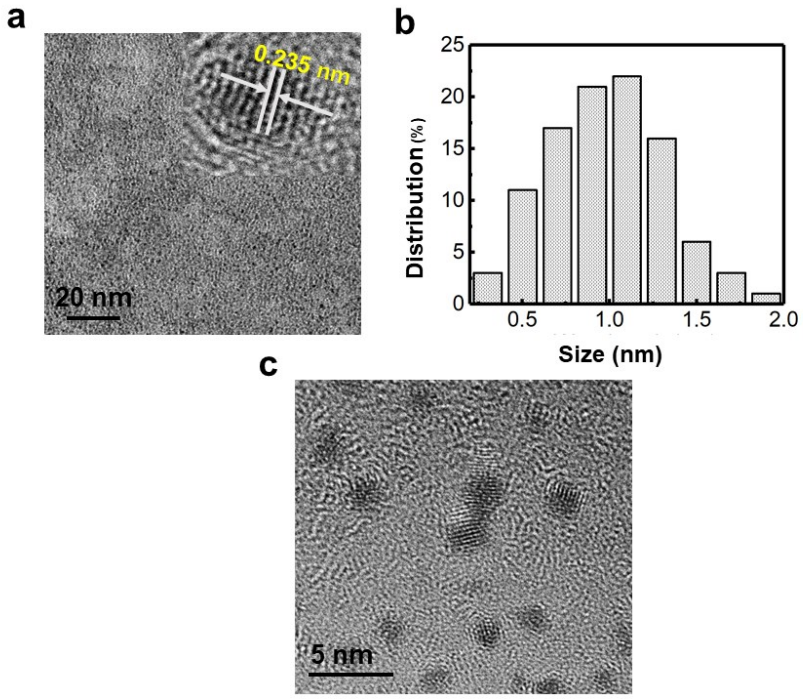

Figure S2 (a) Low magnification transmission electron microscopy (TEM) image, showing small size (ca. 1.1 nm) GSH-AuNCs; The inset of (a) shows well-resolved lattice fringes with measured spacing value "d" value of AuNCs. (b) The size distribution of GSH-AuNCs measured based on the statics of 100 particles. (c) Higher magnification TEM image, which reveals the lattice of the AuNCs.

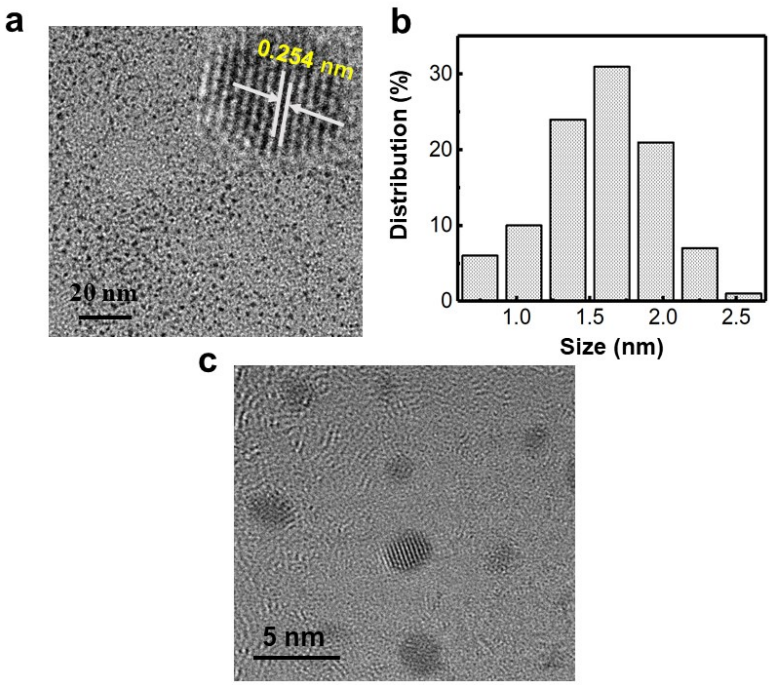

Figure S3 (a) Low magnification transmission electron microscopy (TEM) image, showing small size (ca. 1.6 nm) DHLA-AgNCs; The inset of (a) show well-resolved lattice fringes with measured spacing value "d" value of AgNCs. (b) The size distribution of DHLA-AgNCs measured based on the statics of 100 particles. (c) Higher magnification TEM image, which reveals the lattice of the AgNCs.

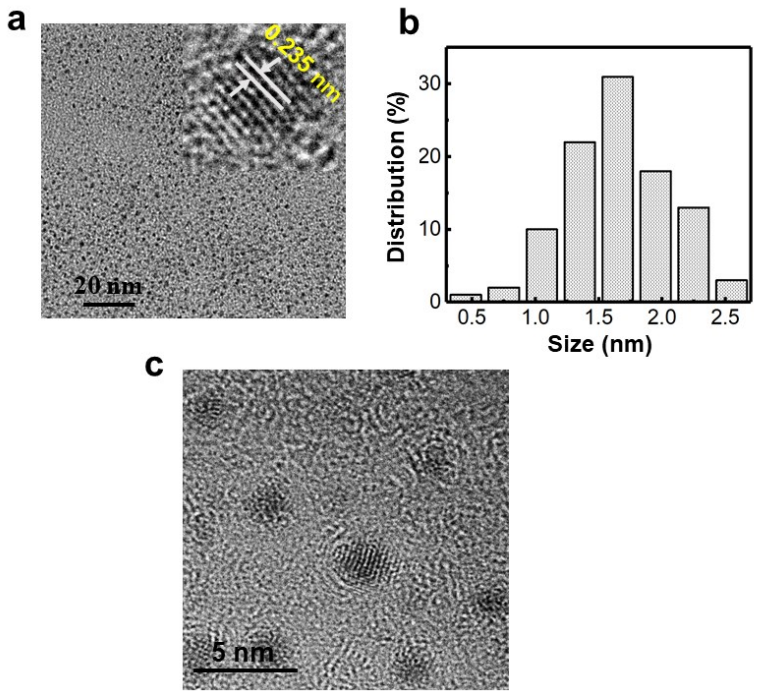

Figure S4 (a) Low magnification transmission electron microscopy (TEM) image, showing small size DHLA-AuNCs (ca. 1.6 nm); The inset of (a) show well-resolved lattice fringes with measured spacing value "d" value of AuNCs. (b) The size distribution of DHLA-AuNCs measured based on the statics of 100 particles. (c) Higher magnification TEM image, which reveals the lattice of the AuNCs.

3. DLS of NCs

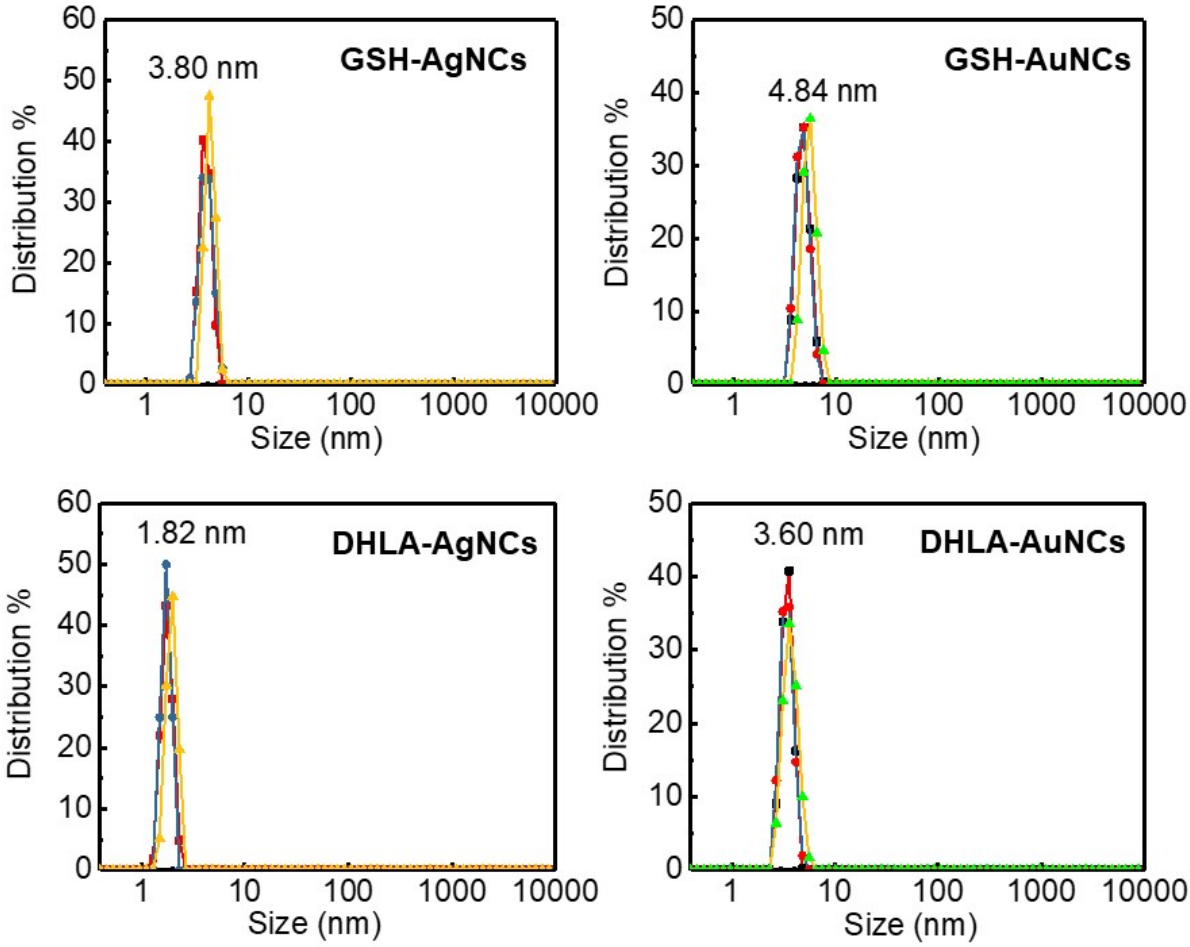

Figure S5 DLS size distribution histogram of GSH-AgNCs, GSH-AuNCs, DHLA-AgNCs, and DHLA-AuNCs.

4. XPS of NCs

The XPS spectrum of AgNCs shows two binding energy values at 368.2 eV for Ag $3d_{5/2}$ and 374.4 eV for Ag $3d_{3/2}$, confirming the presence of elemental Ag(0) in the AgNCs, consistent with the standard spectrum for AgNCs.[1] The $Ag3d_{5/2}$ peaks are observed at relatively higher energy (at ~368.2 eV) compared to Ag(0) (normally located at ~368 eV). This positive energy shift can be attributed to the surface coordination of GSH, which enables the presence of Ag(Ⅰ). Moreover, the XPS survey reveals that O, C, N, S, and Ag that belongs to GSH and Ag Core, are present in the sample, which confirms the formation of GSH-AgNCs.

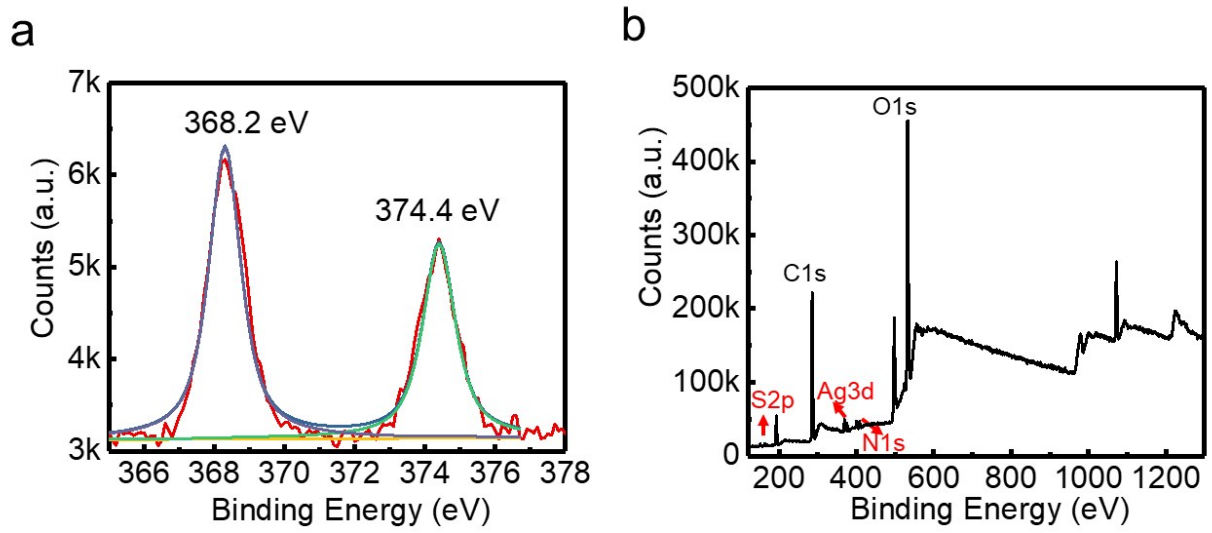

Figure S6 Ag XPS spectra (a) and XPS survey (b) of GSH-AgNCs (one drop of 100 μM dried sample purified by dialysis).

In XPS spectra for GSH-AuNCs, peaks are found at 84.4 eV and 88.1 eV for gold.[2] These peaks correspond to Au $4f_{7/2}$ and Au $4f_{5/2}$, respectively. The positive energy shift of 84.4 eV compared to 84.0 eV for Au(0) can be attributed to the surface coordination of GSH, which indicates the presence of Au(Ⅰ). Moreover, the XPS survey reveals that O, C, N, S, and Au that belong to GSH and Au core respectively, are present in the sample, which confirms the formation of GSH-AuNCs.

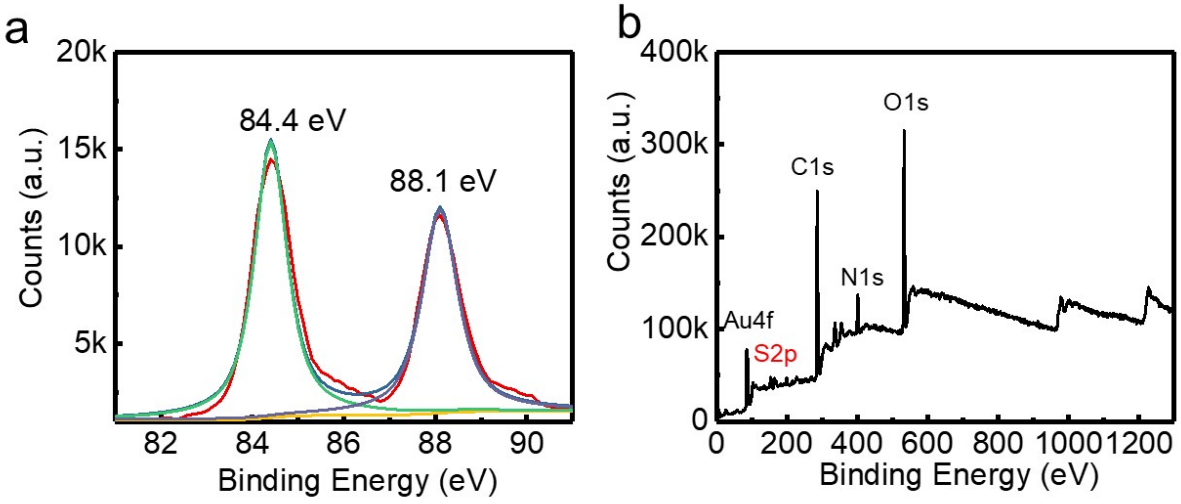

Figure S7 Au XPS spectra (a) and XPS survey (b) of GSH-AuNCs (one drop of 100 μM dried sample purified by dialysis).

Ag peaks at 368.0 and 374.0 eV, corresponding to Ag $3d_{5/2}$ and $3d_{3/2}$ orbital splitting, respectively, confirming the existence of metallic Ag(0) NCs.[3] On the other hand, weak peaks for Ag-O bonds (at binding energies 377 or 371 eV) were observed, indicating few Ag_2O are present due to the oxidation. These results confirmed that the formation of DHLA protected AgNCs and the surface charge is dominated by Ag(0), but few Ag is oxidized as Ag_2O. Moreover, the XPS survey revealed that O, C, S, and Ag that belong to DHLA and Ag core respectively, are present in the sample, which confirms the formation of DHLA-AgNCs.

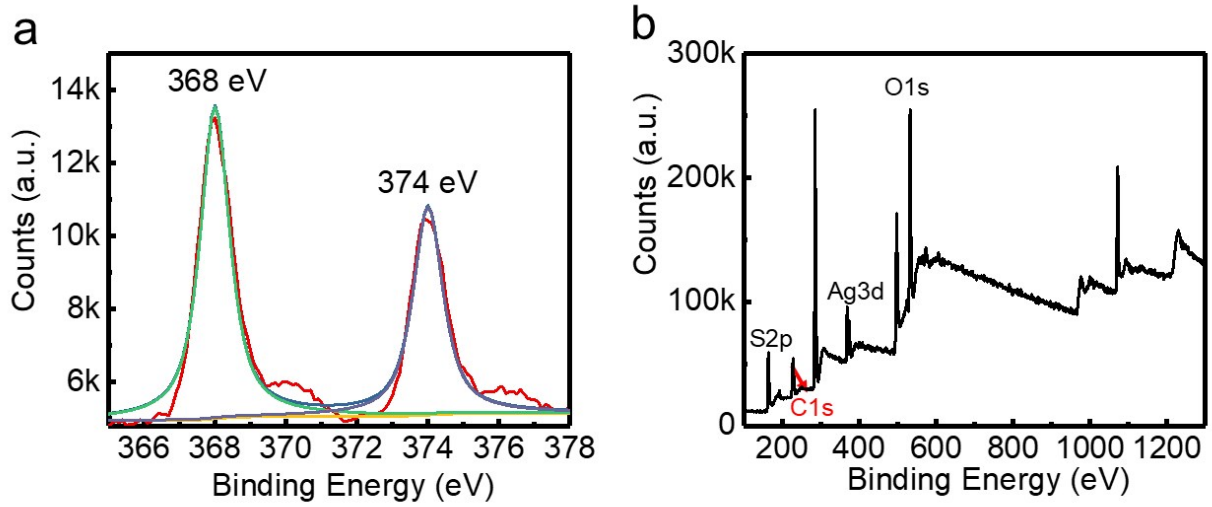

Figure S8 Ag XPS spectra (a) and XPS survey (b) of DHLA-AgNCs (one drop of 100 μM dried sample purified by dialysis).

In XPS spectra for GSH-AuNCs, peaks are found at 84.3 eV and 87.9 eV for gold,[4] which correspond to Au $4f_{7/2}$ and Au $4f_{5/2}$, respectively. The blue shifts in the XPS peak of DHLA-AuNCs compared to GSH-AuNCs are related to the oxidation state and a lower shift in binding energy corresponds to a lower oxidation state. It indicates more Au(0) dominates the surface of DHLA-AuNCs than GSH-AuNCs. The DHLA-AgNCs may be more resistant to be oxidized as oxidized states compared to GSH-AuNCs that have more ratio of Au(Ⅰ) at the surface. Moreover, the XPS survey revealed that O, C, S, and Au that belong to DHLA and Au core respectively, are present in the sample, which confirms the formation of DHLA-AuNCs.

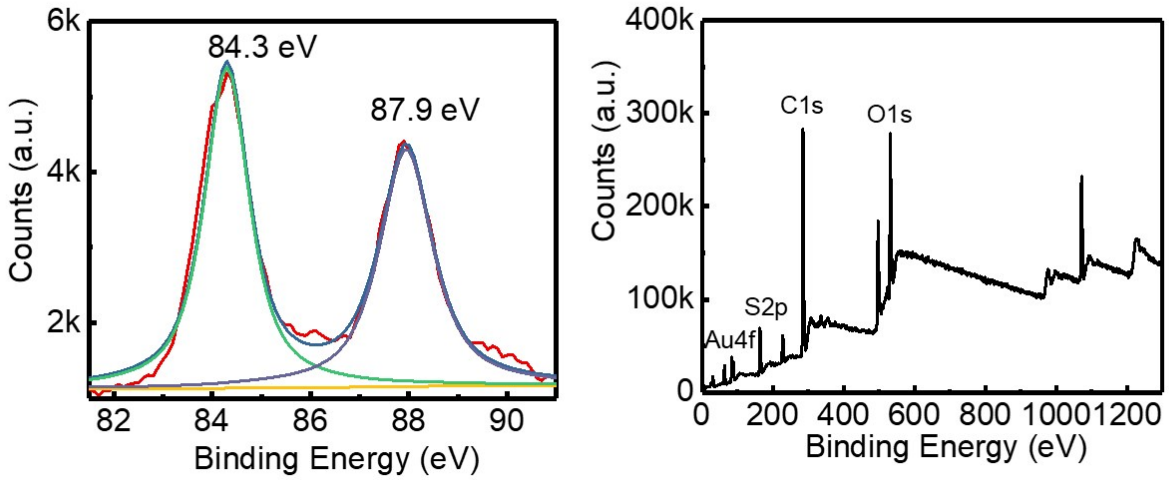

Figure S 9 Au XPS spectra (a) and XPS survey (b) of DHLA-AuNCs (one drop of 100 μM dried sample purified by dialysis).

5. Antibacterial investigation

Both DHLA-AgNCs and GSH-AgNCs have been reported to show high antibacterial activity to variable extents, but DHLA-AuNCs and GSH-AuNCs are not effective for eradication of any types of bacteria. Because bacterial infections will delay wound healing, the antibacterial activity of NCs (100 μM) against typical Gram-negative and Gram-positive bacteria such as *E. coli* and *S. aureus* are investigated by the metabolic power-time curve (Figure S10). The curves are fitting by the following equation:

$$P_t = P_0(kt)$$

where P_0 represents the heat output power when t = 0; P_t represents the power at time t. By simulating the equation, the rate constants (k_1) of the first and the second exponential phase (k_2) for the bacterial growth at 37 ◦C were obtained (Table S1). The rate constants for both AuNC AgNC groups are not significantly different from the control values. As such, the antibacterial effects of NCs with this concentration may not play an important role in wound therapy.

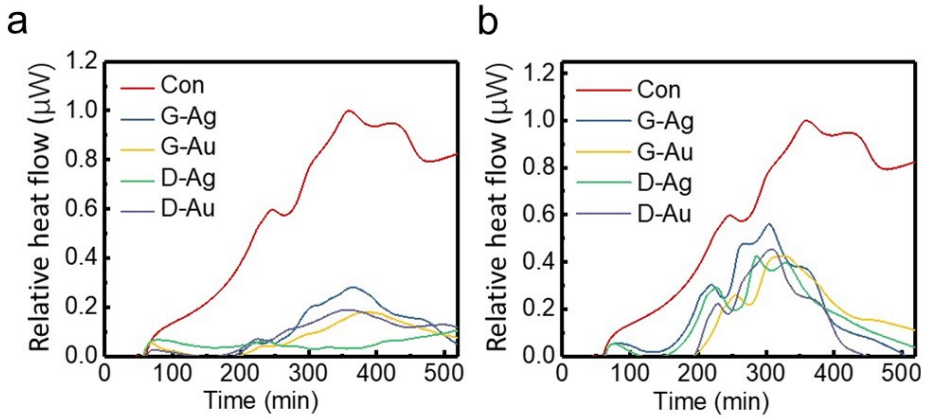

Figure S 10 Growth thermogenic curves of *S. aureus (a) and E. coli* (b) in the absence and presence of NCs (a)). (G-Ag, GSH-AgNCs; G-Au, GSH-AuNCs; D-Ag, DHLA-AgNCs; D-Au, DHLA-AuNCs).

Table S 1 The growth rate constants (k_1 and k_2) of *S. aureus* and *E. Coli*

	S. aureus		***E. Coli***	
Rate Constants	**k_2**	**k_1**	**k_2**	**k_1**
Control	0.0177491	0.0238343	0.0169782	0.0244819
GSH-AgNCs	0.0140016	0.0148608	0.0177833	0.0217734
GSH-AuNCs	0.0122753	0.0137699	0.0157975	0.0181387
DHLA-AgNCs	0.0081204	0.0151304	0.0179384	0.0209211
DHLA-AuNCs	0.0130821	0.0164679	0.0168099	0.0195186

6. Cell-mediated inflammation analysis

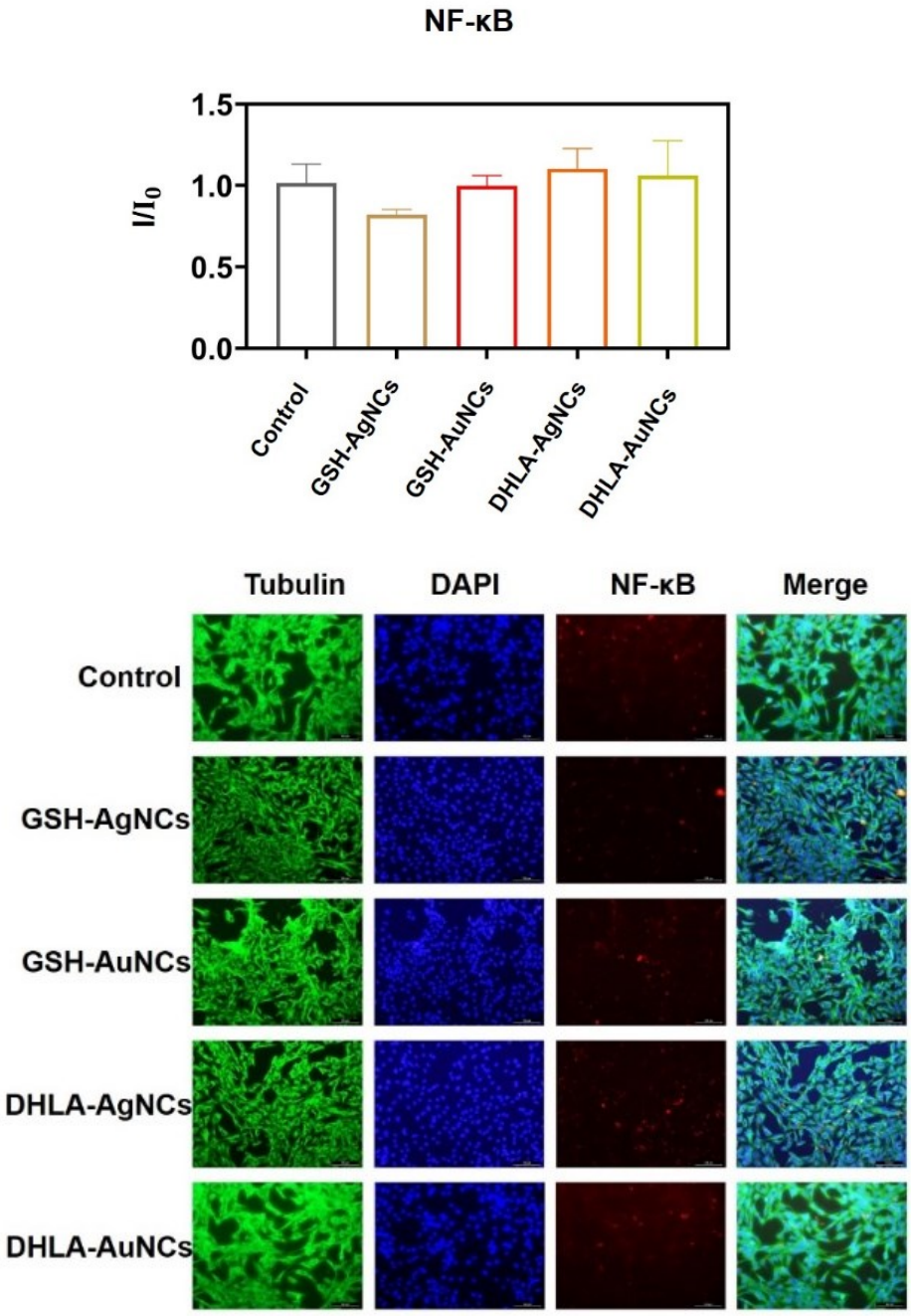

Figure S11 Fluorescence intensity (up) and imaging (down) of NF-κB p65 (NF-κB) in the culture of HUVECs with control, 100 μM of GSH-AgNCs,100 μM of GSH-AuNCs, 100 μM of DHLA-AgNCs, and 100 μM of DHLA-AuNCs. Scale bar: 100 μm.

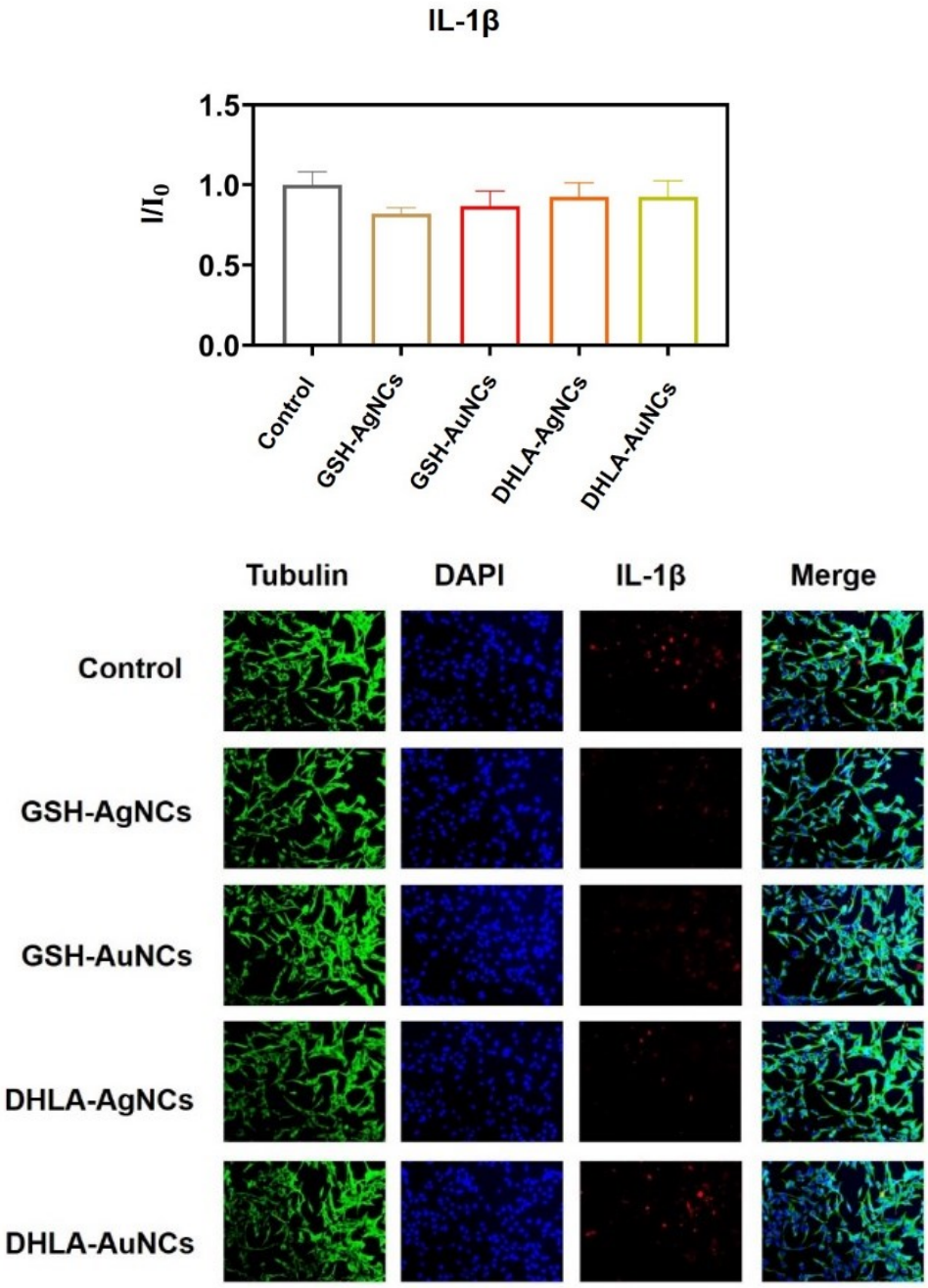

Figure S12 Fluorescence intensity (up) and imaging (down) of IL-1 β in the culture of HUVECs with control, 100 μM of GSH-AgNCs, 100 μM of GSH-AuNCs, 100 μM of DHLA-AgNCs, and 100 μM of DHLA-AuNCs. Scale bar: 100 μm.

7. ROS scavenging capability of AuNCs

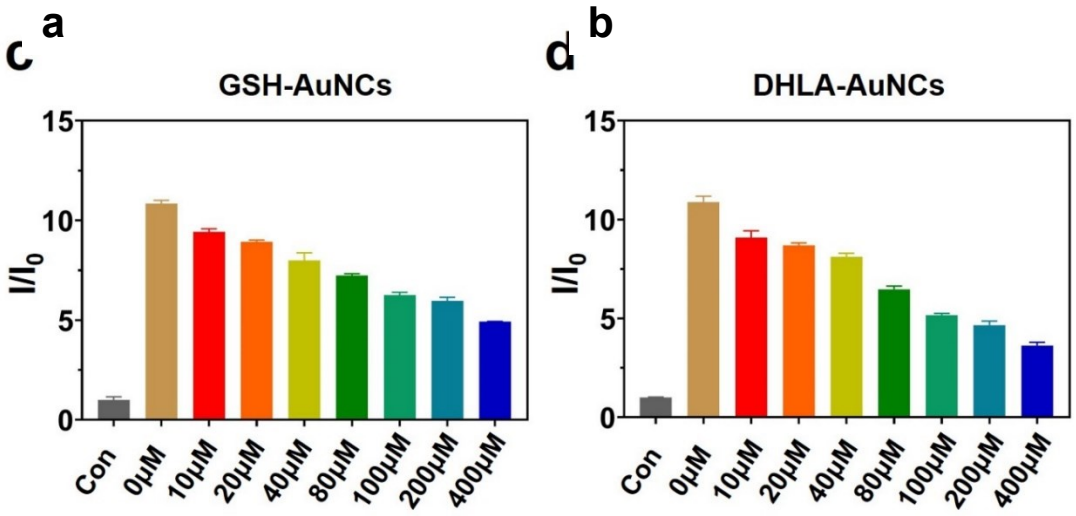

Figure S13 ROS scavenging capability of GSH-AuNCs (a), and DHLA-AuNCs (b). Control (the mixture of H_2O_2 and PB buffer) and DCFH-DA probe with H_2O_2 treated with different concentrations of AuNCs.

Table S2 Evaluation of epidermal regeneration, fibrous tissue regeneration, angiogenesis, and skin appendages during skin wound healing

	Epidermal	Fibrous	Vascular	Skin
Control	+	+	-	-
GSH-AgNCs	+	+	-	-
GSH-AuNCs	+	+	+	+
DHLA-AgNCs	+	+	+	-
DHLA-AuNCs	+	+	++	++

Note: '+' indicate promising and '–' represents less-promising phenomena.

8. Immunological response study

Immunohistochemical staining for CD68 (a macrophage marker) and TGF-β (a marker related to inflammation and scar-forming) were performed in skin tissue sections after injection of NCs on the wound area to evaluate the immunomodulatory effects of NCs. The overexpression of these factors in wounds can lead to inflammation and delayed wound healing. AuNCs-treated tissues demonstrated significantly reduced expression of both TGF-β and CD68. Fewer TGF-β-expressing cells were observed in the AuNCs conditions compared with those of the AgNCs and control group. This indicates that the AuNCs can decrease inflammatory conditions.

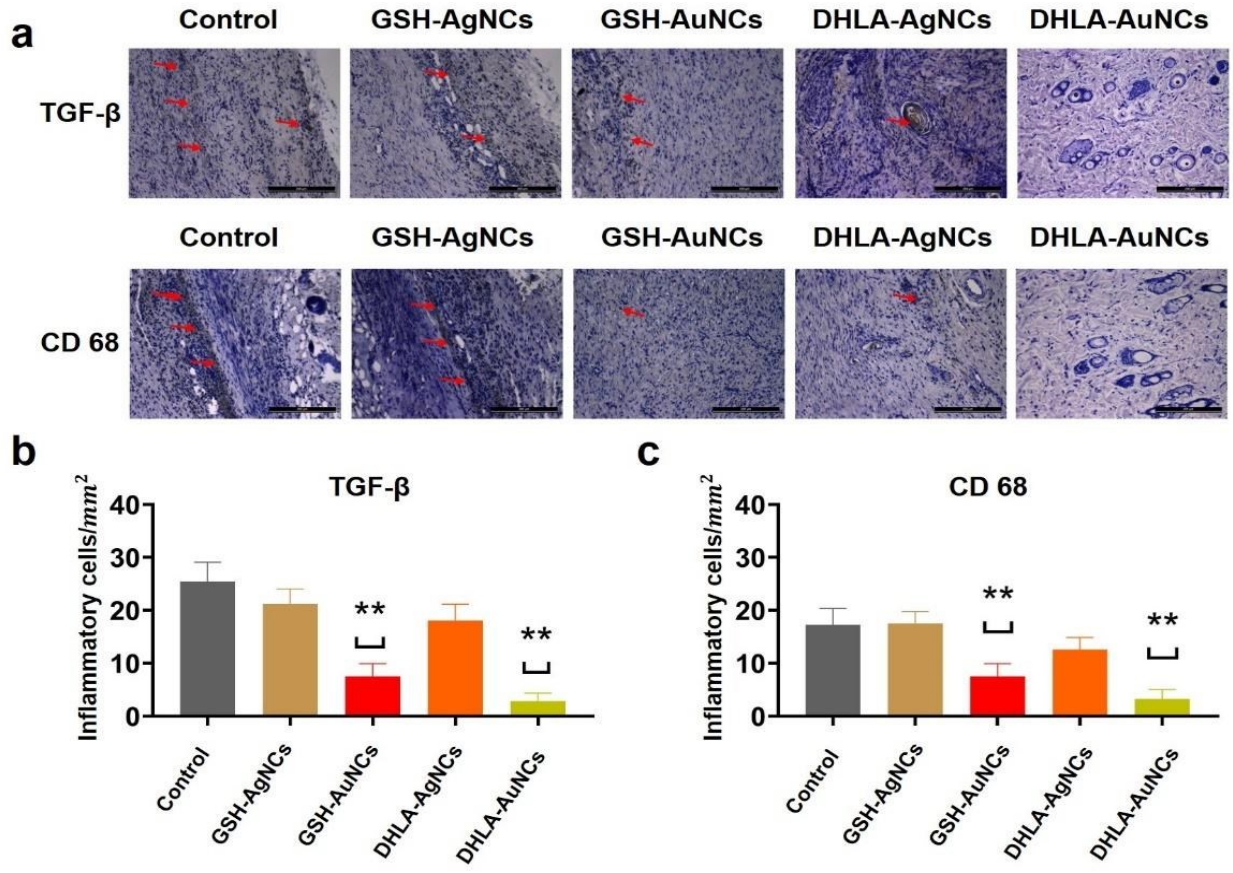

Figure S14 Immunostaining of CD68 and TGF-β in skin tissue sections after injection of NCs. (a) TGF-β and CD68 immunohistochemical staining and inflammatory cell-related counts positive for TGF-β (b) and CD68 (c) staining. Red arrow indicates a positive expression. * indicates a statistically significant difference, $P < 0.05$. The bar is 200 μm.

Cytokine analysis

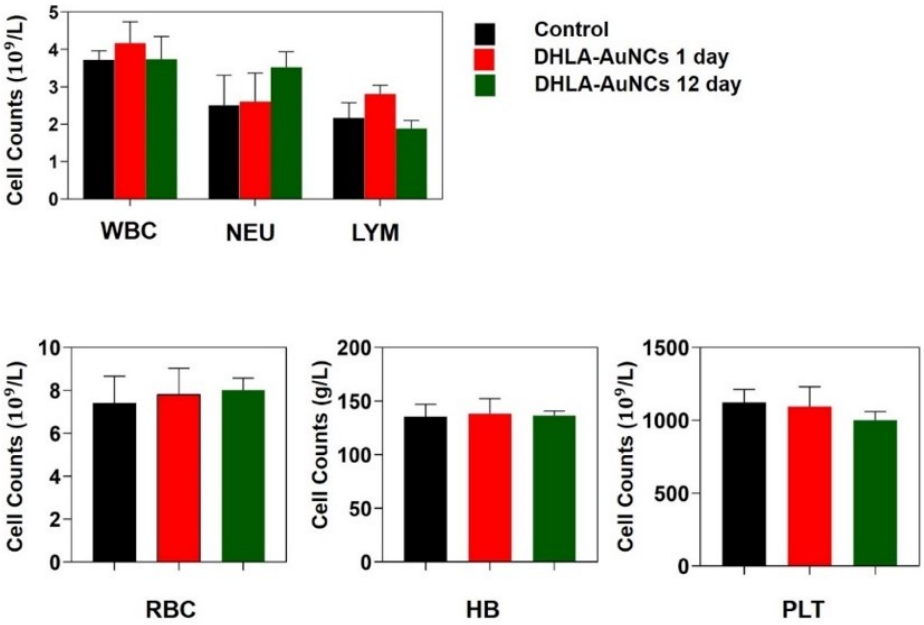

	WBC	NEU	LYM
		10^9/L	
Control	3.72±0.20	2.51± 0.65	2.16±0.34
DHLA-AuNCs 1 day	4.17±0.47	2.61± 0.62	2.81±0.19
DHLA-AuNCs 12day	3.74 ±0.50	3.52± 0.34	1.88±0.18
Reference	2.85-9.59	0.1-5.8	0.75-5.7

	RBC	HB	PLT
	10^{12} /L	g/L	10^9/L
Control	7.43±1.01	135.33±9.46	1123.55±72.18
DHLA-AuNCs 1 day	7.80±1.00	138.33±11.44	1094.54±110.76
DHLA-AuNCs 12day	8.01±0.46	136.33±3.68	999.68±48.80
Reference	8.01±0.46	123.75-152.23	961.47-1215.39

Figure S15 The blood routine test of rat treated with DHLA-AuNCs after different days. (up) The comparison for the cell amounts and (down) the detailed data for the blood routine test. Note: (WBC: white blood cell; NEU: neutrophilic granulocyte; LYM: lymphocyte; RBC: Red blood cell; HB: hemoglobin; PLT: platelet count; Reference: Normal range.

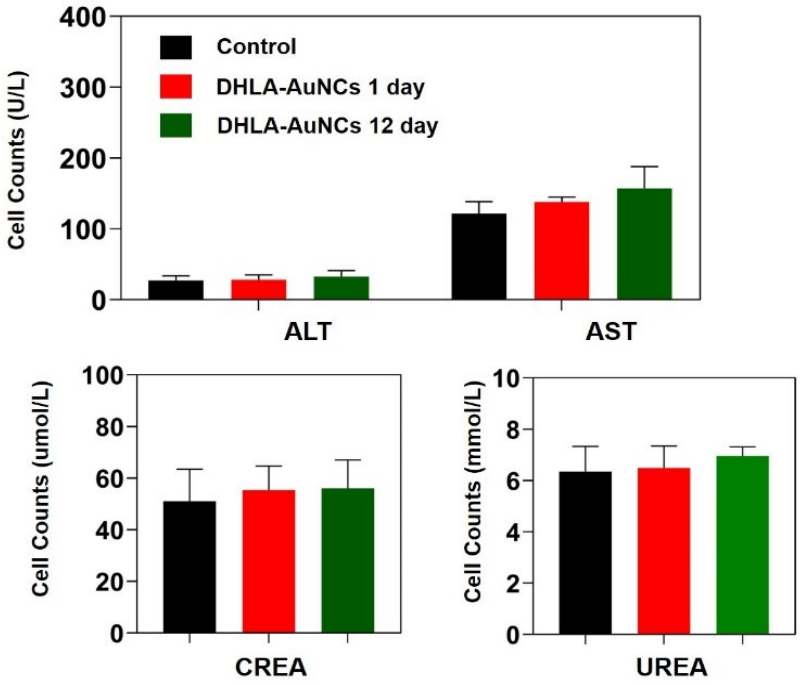

	ALT	AST	CREA	UREA
	U/L	U/L	Umol/L	mmol/l
Control	27.33±5.31	121.33±13.89	51.00±10.17	6.36±0.79
DHLA-AuNCs 1 day	28.33±5.56	138.00±5.66	55.33 ±7.59	6.49±0.70
DHLA-AuNCs 12day	32.67±6.85	157.00 ±25.15	56.03±8.94	6.96±0.29
Reference	22.50-43.70	81.52-190.66	36.78-67.08	4.30-9.78

Figure S16 The blood routine test of rat treated with DHLA-AuNCs after different days. (up) The comparison for the cell amounts and (down) the detailed data for the blood routine test. Note: (ALT: Alanine aminotransferase; AST: Aspartate Aminotransferase; CREA: creatinine; UREA: urea); Reference: Normal range.

9. Clearance study

A biodistribution analysis was performed by collecting organ samples at various time points for a total of 48 hours and assessing tissue gold content using inductively coupled plasma mass spectrometry (ICP-MS). The majority of relatively large particles tend to accumulate in the liver and spleen.[5] However, we observed a substantial drop in gold levels after the injection of DHLA-AuNCs in different organs over a short time. On average, gold is decreased dramatically over 6 hours. The clearance is rapid and efficient, which compare favorably to those large nanomaterials reported in various studies.[6-7]

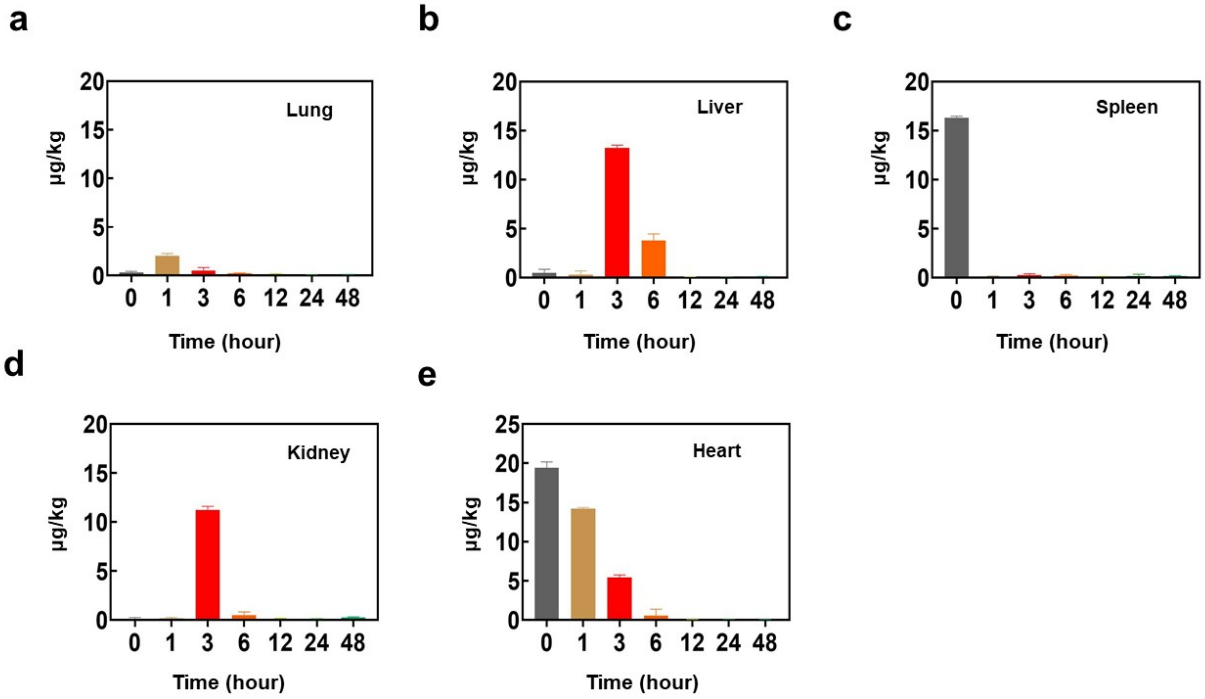

Figure S17 The presence of gold in major organs including lung (a), liver (b), spleen (c), kidney (d), and heart (e) as a function of time. The DHLA-AuNCs were injected intraperitoneally with a dose of 0.2 ml of 100 μM. Note: Ratio = C/C_0; Where C_0 and C indicate the original concentration of Au and the concentration after certain hours.

References

[1] A. Aires, I. Llarena, M. Moller, J. Castro-Smirnov, J. Cabanillas-Gonzalez and A. L. Cortajarena, *Angew Chem Int Ed Engl*, 2019, **58**, 6214-6219.

[2] J. Jana, T. Aditya and T. Pal, *New Journal of Chemistry*, 2019, **43**, 7074-7082.

[3] D. Mishra, V. Lobodin, C. Zhang, F. Aldeek, E. Lochner and H. Mattoussi, *Phys Chem Chem Phys*, 2018, **20**, 12992-13007.

[4] C. Zhou, C. Sun, M. Yu, Y. Qin, J. Wang, M. Kim and J. Zheng, *J Phys Chem C Nanomater Interfaces*, 2010, **114**, 7727-7732.

[5] A. A. Elizabeth M. Higbee-Dempsey, Matthew J. Case, Mathilde Bouche, Johoon Kim,´David P. Cormode, Andrew Tsourkas, *J. Am. Chem. Soc.*, 2020, **142**, 7783−7794.

[6] X. D. Zhang, D. Wu, X. Shen, P. X. Liu, F. Y. Fan and S. J. Fan, *Biomaterials*, 2012, **33**, 4628-4638.

[7] X. Zhang, X. Guo, X. Kang, H. Yang, W. Guo, L. Guan, H. Wu and L. Du, *Chem Res Toxicol*, 2020, **33**, 1195-1205.